

# Observation of the Quantum Zeno Effect on a Single Solid State Spin

Janik Wolters,<sup>1,\*</sup> Max Strauß,<sup>1</sup> Rolf Simon Schoenfeld,<sup>1</sup> and Oliver Benson<sup>1</sup>

<sup>1</sup>*Nano-Optics, Institute of Physics, Humboldt-Universität zu Berlin, Newtonstr. 15, D-12489 Berlin, Germany*

The quantum Zeno effect, i.e. the inhibition of coherent quantum dynamics by projective measurements is one of the most intriguing predictions of quantum mechanics. Here we experimentally demonstrate the quantum Zeno effect by inhibiting the microwave driven coherent spin dynamics between two ground state spin levels of the nitrogen vacancy center in diamond nano-crystals. Our experiments are supported by a detailed analysis of the population dynamics via a semi-classical model.

It was no later than 430 BC, when ancient greek's philosopher Zeno of Elea formulated his well known arrow paradox [1]. If an object can be observed at any instance of time to be at a well defined position in space motion can not occur. It took over 2 millennia until I. Newton and G.W. Leibniz solved the paradox with the invention of infinitesimal calculus. Then, in 1977 it was shown that the paradox rises again from the formalism of quantum mechanics [2]. If a quantum system is permanently observed, its coherent dynamics can be significantly slowed down and eventually even frozen. Later on, the group of the 2012's Nobel laureate D.J. Wineland observed this so-called quantum Zeno effect in the radio frequency transition between two  $^9\text{Be}^+$  ground-state hyperfine levels [3]. Aside from philosophic implications of the phenomenon, recent proposals aim towards technologically utilizing the broader formulated quantum Zeno dynamics [4] for efficient quantum gates and fault tolerant quantum operation [5–7]. In this letter, we demonstrate the quantum Zeno effect in a solid state spin, namely the ground state spin of a single negatively charged nitrogen vacancy (NV) center in diamond. Beyond its analogy to a classical paradox the quantum Zeno effect here allows for a detailed study of the intricate interplay of coherent and incoherent dynamics of a single quantum system interacting with a macroscopic environment [8].

The NV center is one of the most studied color centers in diamond and single NV centers have proven to be excellent solid state quantum systems. They are frequently used as single photon source [9, 10], spin qubit [11–13], or bio-compatible sensors [14]. Nanodiamonds can be integrated into various other systems like cells, photonic crystal structures [15–17] or plasmonic elements [18, 19]. The origin of this versatility is a combination of the NV center's level structure, excellent ground state spin coherence and stability of the diamond host lattice [11, 20]. The electronic level structure according to the NV center's  $c_{3v}$ -symmetry is depicted in Fig. 1 (b) [21, 22]. The level structure consists of a triplet ground state  $^3A_2$  with the spin  $m_s = 0$  sub-level  $S_z A_1$ , and the  $m_s = \pm 1$  states  $S_{x,y} A_1$ . At zero magnetic field the  $m_s = \pm 1$  states are split from the  $m_s = 0$  level by approximately 2.9 GHz. The triplet excited state  $^3E$  has the two-fold

degenerate  $m_s = 0$  sublevels  $S_z E_{x,y}$ , while the  $m_s = \pm 1$  manifold is given by the four-fold degenerate  $S_{x,y} E_{x,y}$ . Using off-resonant excitation by a 532 nm laser levels of same spin can be linked by spin-preserving optical transitions at approximately 638 nm with the excitation rate  $k_{exc}$  and radiative decay rate  $k_{rad}$ , assumed to be equal for all spin states. Furthermore, two singlet states  $^1A_1$  and  $^1E$  exist. The state  $^1A_1$  can be reached via inter system crossing (ISC) from the  $m_s = \pm 1$  manifold and decays via  $E_1$  to the  $m_s = 0$  ground state as indicated by the dashed arrows in Fig. 1 (b).

Via this ISC process the NV center is efficiently polarized within a few excitation-decay cycles. Furthermore, since the deshelling rate from  $E_1$  to the  $S_z A_1$  ground state is comparably low the spin dependent ISC process makes the  $m_s \pm 1$  states appear darker than the  $m_s \pm 0$  counterpart, enabling the optical detection of the magnetic resonance (ODMR). These spin detection and initialization mechanisms combined with long coherence times in the mainly spin-free diamond lattice render the NV center ideal to demonstrate coherent spin manipulation by microwaves. For example electromagnetic induced transparency [23], simple quantum algorithms [24] and subdiffraction optical magnetometry [25] have been demonstrated. In Refs. [23, 25] a 532 nm laser is

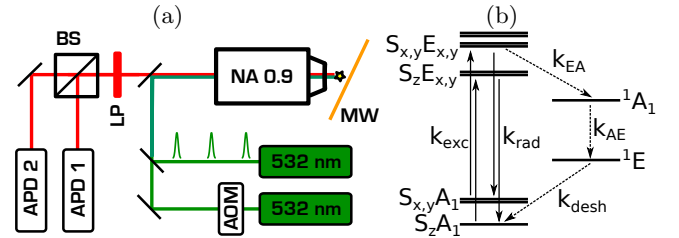


FIG. 1. (Color online) (a) The optical setup. Individual NV centers are excited by a pulsed 532 nm laser or a 532 nm cw laser modulated by an acousto-optic modulator (AOM) through a high NA objective lens. Fluorescence is separated by a dichroic mirror and an additional long pass filter (LP) prior to detection by a Hanbury-Brown and Twiss setup consisting of two avalanche photo diodes (APD) and a beam splitter (BS). Additionally, microwave pulses can be applied via a thin gold wire in the vicinity of the diamond nano-crystals (MW). (b) Schematic level diagram of the NV center without strain. See text for details.

used to inhibit a population transfer from the  $m_s = 0$  to  $m_s = +1$  ground state, but it remains speculative, whether this is due to the quantum Zeno effect, or classical repumping into the  $m_s = 0$  state. In this letter, we address this question experimentally, as well as by numerical simulations. For this purpose, at first the population dynamics of the investigated NV center are determined. In a second step, we use a pulsed 532 nm laser to inhibit the coherent microwave driven population transfer between the  $m_s = 0$  and  $m_s = 1$  ground state. Our results are supported by numerical simulations based on the previously determined parameters. Importantly, we demonstrate bidirectional inhibition of the population transfer, i.e. also for the transition from  $m_s = 1$  to  $m_s = 0$ . In this case, classical repumping into the  $m_s = 0$  state contradicts the effect, giving clear evidence for the existence of the quantum Zeno effect in this solid state spin system.

In our experiment, we spin-coated commercial diamond nanocrystals with an average size of 50 nm (*microdiamant AG*) onto a cleaned glass cover slip. Using a homebuilt confocal microscope (NA = 0.9) with Habury-Brown and Twiss setup a single NV center was identified. To perform the spin manipulation, microwaves pulses (MW) could be applied via a gold wire in the vicinity of the sample, while a small permanent magnetic field was used to split up the  $m_s = \pm 1$  spin levels by approximately 250 MHz. In the investigated nanodiamonds

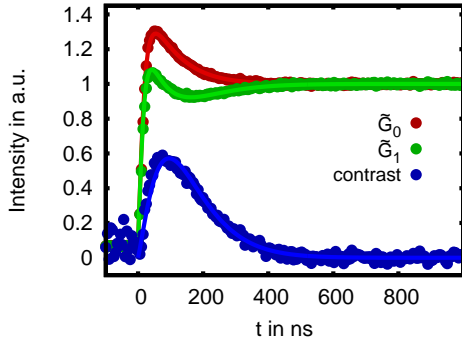


FIG. 2. Fluorescence intensities  $I_{G_{0(1)}}(t)$  of the NV center after switch-on of the cw laser when either the predominantly  $m_s = 0$  state  $\tilde{G}_0$  or the  $m_s = 1$  state  $\tilde{G}_1$  was initially prepared. The contrast defined by  $(I_{G_0} - I_{G_1})/(I_{G_0} + I_{G_1})$  is scaled up by a factor of 5 for better visibility. The solid curves are numerical solutions of the rate equations corresponding to the level diagram depicted in Fig. 3.

magnetic splitting and transition rates vary for different centers due to strain and orientation. Thus, several measurements were performed to gain insight into the specific level-structure and dynamics. First, the well established ODMR technique [23] was used to identify the ground state spin resonances. Subsequently, coherent Rabi oscil-

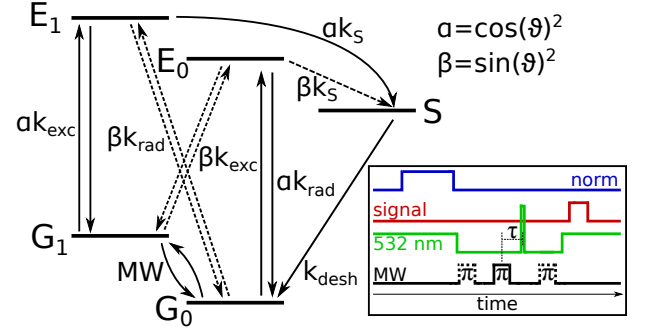


FIG. 3. Simplified level diagram and transition rates of the NV center with strain. The  $m_s = 0(1)$  electronic ground state is denoted  $G_{0(1)}$ , while the corresponding predominantly  $m_s = 0(1)$  excited states are  $E_{0(1)}$ . The singlet states are merged to the state S. Solid arrows correspond to allowed transitions, while dashed arrows indicate forbidden transitions. The microwave induced coherent ground state spin rotations are indicated by MW. The inset shows the pulse sequence used to measure the Zeno effect. MW denotes the microwave source used to apply up to 3  $\pi$ -pulses. The 532 nm cw laser is used to initialize the NV center at the beginning of the experiment and for state readout at the end, while a strong pulse from the pulsed laser is applied at time delay  $\tau$  with respect to the center of the central  $\pi$ -pulse. The NV fluorescence intensity is measured within short time windows after and prior to applying the  $\pi$ -pulses to obtain the signal and normalization reference as indicated.

lations were driven to measure the oscillation frequency  $\Omega$ , as well as the damping of the oscillation  $1/T_2$  (cf. Supplemental Material). To estimate the transition rates between different levels, first the  $m_s = 0$  state was prepared by applying a green cw laser (1.2 mW) for of about 5  $\mu$ s (cf. Fig. 1 (a)). About 2  $\mu$ s after switching off the laser the NV center is assumed to be relaxed into the desired  $m_s = 0$  state, which can be transformed into the  $m_s = 1$  state by an optional MW  $\pi$ -pulse. Subsequently the time dependent fluorescence intensity after switching on the cw laser again was measured (Fig. 2). These dynamics strongly depend on the transition rates between different levels. To estimate these transition rates, we have to remark that strain induces a mixing of excited states with different spin orientations by the angle  $\vartheta$ , resulting in the model depicted in Fig. 3, where we denote the predominantly  $m_s = 0(1)$  excited state  $E_{0(1)}$ . The mixing has two direct implications: Spin non-preserving optical transitions, as well as inter-system crossing from the predominantly  $m_s = 0$  excited state become possible [26, 27]. According to Fermi's golden rule the rates of the transition allowed in the unstrained NV are reduced by the factor  $\cos(\vartheta)^2$ , whereas the formally forbidden transitions have now the rates  $k_x \sin(\vartheta)^2$ , with  $k_x$  being the rate of the corresponding allowed transition. To simplify the model, we do not consider the  $m_s = -1$  manifold and merge the singlet states to the single deshelling state S. A differential equation repre-

sensation of the model can be found in the Supplemental Information. Using this model the measured dynamics can be exactly reproduced (solid line in Fig. 2). A summary of the deduced rates is given in Table 1. A first important consequence of the model is a reduced polarization efficiency  $\eta_{pol}$ . By illumination with green light the bright state  $\tilde{G}_0 = \eta_{pol}G_0 + (1 - \eta_{pol})\exp(i\varphi_1)G_1$  with random phase  $\varphi_1$  is prepared. A subsequent microwave  $\pi$ -pulse transfers the population into the dark state  $\tilde{G}_1 = \eta_{pol}G_1 + (1 - \eta_{pol})\exp(i\varphi_2)G_0$ . For additional verification of the deduced parameters, we independently measured the excited states lifetimes with a pulsed laser (PicoQuant LDH-P-FA-530-XL), deduced the excitation rate  $k_{exc}$  from saturation measurements and the derived contribution of fluorescent background to the signal  $I_{bg}$  from autocorrelation measurements. All parameters were consistent with those deduced from the fit.

TABLE I. Transition rates and parameters deduced by fitting the model (Fig. 3) to the measurement shown in Fig. 2. The error corresponds to one standard deviation confidence interval.

$2\pi/\Omega$	$(80.0 \pm 0.5) \text{ ns}$
$T_2$	$(1.0 \pm 0.5) \mu\text{s}$
$1/k_{exc}$	$(33.5 \pm 5) \text{ ns}$
$1/k_{rad}$	$(34 \pm 5) \text{ ns}$
$1/k_{desh}$	$(146 \pm 9) \text{ ns}$
$1/k_S$	$(38 \pm 5) \text{ ns}$
$\vartheta$	$(20.1 \pm 1.7)^\circ$
$I_{bg}$	$0.09 \pm 0.09$
$\eta_{pol}$	$0.85 \pm 0.01$

After determining the transition rates the quantum Zeno experiment was simulated and experimentally realized. The experimental sequence is illustrated in the inset of Fig. 3. First, the NV center is initialized to the bright state  $\tilde{G}_0$  by applying the green cw laser for about 5  $\mu\text{s}$ . In order to initialize the dark  $\tilde{G}_1$  state a subsequent MW pulse can be applied for a length of 40 ns. This corresponds to a  $\pi$ -pulse and transfers the population from  $\tilde{G}_0$  to  $\tilde{G}_1$ . After the initialization the MW pulse is switched on starting a coherent transition from  $\tilde{G}_0$  to  $\tilde{G}_1$  (or from  $\tilde{G}_1$  to  $\tilde{G}_0$ ). The pulse is set to a fixed length of 40 ns, i.e. a  $\pi$ -pulse. Synchronized to the microwave pulse, a strong green laser pulse from the pulsed laser (pulse energy about 350 pJ) is applied at varying time delay  $\tau$ . This laser pulse performs a projective measurement of the NV center's spin state, although the generated photons are not detected. Finally, about 300 ns after the microwave pulse the green cw laser is turned on again and the fluorescence of the NV is recorded, giving a measure of the remaining population in the brighter  $G_0$  state. Fig. 4 shows the detected intensity (dots) and numerical simulations (solid). Dashed vertical lines indicate

the switch-on and switch-off of the MW pulse. Quantum theory predicts, that the strong projective laser pulse destroys the microwave induced coherent polarization, and thereby inhibits the dynamics. This process depends on the time delay between the laser and the MW pulse. At the center of the MW-pulse the polarization reaches its maximum (cf. Supplemental Material). Hence a projective laser pulse at  $\tau = 0$  effectively inhibits further coherent dynamics and the final state has a large component of the initial state. This behavior is clearly visible in Fig. 4(a) as increased (decreased) fluorescence around  $\tau = 0$  when the initial state was  $\tilde{G}_0$  ( $\tilde{G}_1$ ). The experimental results are well reproduced by the numerical simulation based on the previously determined parameters. In particular, the decreasing intensity for an initial  $\tilde{G}_0$  at positive values of  $\tau$  in Fig. 4 (a), i.e. when the NV is in the dark state  $\tilde{G}_1$  when the strong laser pulse is applied, proves that the effect is not due to repumping of the NV center.

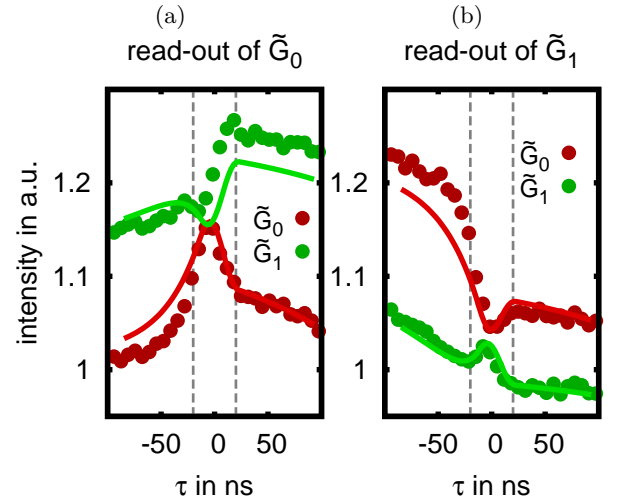


FIG. 4. Measurement (dots) and numerical simulation (solid lines) of the NV fluorescence after the quantum Zeno experiment. (a) The NV center is initialized to the bright  $\tilde{G}_0$  (dark  $\tilde{G}_1$ ) state. The coherent population transfer during the MW pulse (indicated by dashed lines) is inhibited by a strong green laser pulse at time delay  $\tau$  with respect to the center of the MW pulse. Subsequently, the fluorescence as a measure of the occupation of the bright state  $\tilde{G}_0$  is probed. As predicted by the numerical simulation (solid curve), the Zeno pulse is most effective at  $\tau = 0$ . (b) Same as (a), but with an additional  $\pi$ -pulse before measuring the NV fluorescence, i.e. monitoring of the population of the dark state  $\tilde{G}_1$ .

To further support this interpretation, we repeated the experiment with an additional  $\pi$ -pulse before measuring the NV fluorescence. This swaps the population of the dark and bright state, i.e. the measured intensity is proportional to the population of the dark state  $\tilde{G}_1$  (Fig. 4 (b)). Again, as predicted by the simulation (solid curve), the transition is most effectively inhibited when the projective laser pulse is applied in the center

of the microwave  $\pi$ -pulse. Here the curve for an initial  $\tilde{G}_1$ , where the coherent spin rotation from  $\tilde{G}_1$  to  $\tilde{G}_0$  is inhibited by the laser, is particularly remarkable. In this configuration the laser pulse effectively *increases* the population of the  $\tilde{G}_1$  state, resulting in an increased fluorescence intensity when probing. To get further insight, we

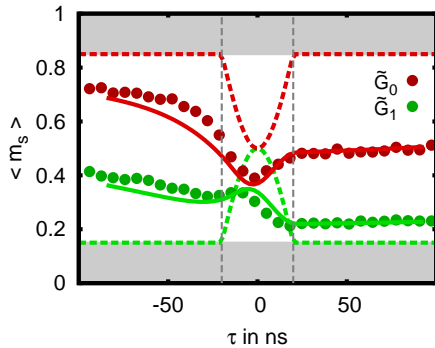


FIG. 5. Experimental values (dots) and numerical simulation (solid curves) of the  $m_s$  spin projection when initially preparing the predominantly  $m_s = 0(1)$  level. Time interval between the vertical lines corresponds to the MW pulse, while the shaded areas are inaccessible due to imperfect polarization. The features centered at  $\tau = 0$  are whiteness of the Zeno effect. Dashed lines indicate the expectations for the ideal case, where the laser pulse destroys the coherence without altering the populations.

calculated the spin projection  $\langle m_s \rangle$  from the contrast between the intensity without final  $\pi$ -pulse (Fig. 4(a)) and the intensity with final  $\pi$ -pulse (Fig. 4(b)). After preparation of the initial state the polarization efficiency is  $\eta_{pol} = 0.85$  as found from fitting the data (Fig. 2) to the model (Fig. 3). Therefore we set  $\langle m_s \rangle = 0.15$  to correspond to the contrast after preparation of  $\tilde{G}_0$ , while  $\langle m_s \rangle = 0.85$  corresponds to the contrast after preparation of  $\tilde{G}_1$ . For the ideal case, where the laser pulse destroys the coherence without altering the populations, a laser pulse not overlapping with the MW pulse should have no influence, i.e. the initial population is completely swapped. A laser pulse within the MW pulse inhibits the coherent dynamics so that at  $\tau = 0$  at most 50% population swapping is reached. The deviation of measurement and realistic simulation from this ideal case (cf. Fig. 5) has several reasons. These are a limited  $T_2$  time, repolarization, and a finite lifetime of the excited states. The first one damps the Rabi oscillations, resulting in a small offset towards  $\langle m_s \rangle = 0.5$ , particularly visible at the curve for an initial  $\tilde{G}_0$  for negative  $\tau$  and for positive  $\tau$  at the curve for an initial  $\tilde{G}_1$ . Repolarization is effective when the NV state has a large  $G_1$  component at time  $\tau$ . This drives the spin towards  $\langle m_s \rangle = 0$  for positive (negative)  $\tau$  in case of initial preparation of  $\tilde{G}_0$  ( $\tilde{G}_1$ ). The finite lifetime of the NV excitation is an issue, when the laser pulse is applied before

the end of the microwave pulse, i.e. for  $\tau < 20$  ns. The laser pulse drives the NV to the excited states, where the MW pulse is ineffective. Consequently this effect is most relevant when the laser pulse is applied immediately before the MW pulse at  $\tau = -20$  ns, while it gets less relevant for smaller or larger  $\tau$ . The behavior is governed by the excitation lifetime  $\tau_{exc}$  and is proportional to  $1 - \exp(\tau/\tau_{exc})$  for  $\tau < -20$  ns. Within the MW pulse ( $-20 \text{ ns} < \tau < 20 \text{ ns}$ ) the shape is given by  $\exp(\tau/\tau_{exc})$ . For initial  $\tilde{G}_0$  the excitation lifetime  $\tau_{exc}$  is on the order of  $\tau_{exc} \approx 1/k_{rad}$  while for an initial  $\tilde{G}_1$  the branching ratio into the metastable singlet S is much larger giving a excitation lifetime  $\tau_{exc} \approx 2/(k_{rad} + k_{desh})$ . This influence of the finite excitation lifetime can well explain the decrease at  $\tau < -20$  ns in the curve for initial  $\tilde{G}_0$ , but does neither explain the shape nor position of the feature at  $\tau = 0$ . This feature is caused by the destruction of the quantum coherence by the strong measurement pulse, i.e. the Zeno effect.

In conclusion we have demonstrate that a strong laser pulse represents a projective measurement of the spin-state of single NV center. A microwave-driven coherent time evolution can be inhibited in this way, representing the quantum Zeno effect in a solid-state system. A model including realistic and experimentally confirmed parameters was derived to explain the quantum Zeno dynamics in detail. Future work will be devoted to the demonstration of the quantum Zeno effect under spin selective optical excitation, e.g. at cryogenic temperature. Here the effect will not only be more pronounced, but is also relevant for recently proposed robust two-qubit quantum gates [5–7].

This work was supported by the DFG (FOR 1493). J. Wolters acknowledges funding by the state of Berlin (Elsa-Neumann). We thank PicoQuant GmbH for collaboration and support.

\* Electronic mail: janik.wolters@physik.hu-berlin.de

<sup>1</sup> Aristotle. Physics. In *Book VI*.

<sup>2</sup> B. Misra and E. C. G. Sudarshan. *J. Math. Phys.*, **18**, 756, (1977).

<sup>3</sup> W. Itano, D. Heinzen, J. Bollinger, and D. Wineland. *Phys. Rev. A*, **41**, 2295 (1990).

<sup>4</sup> P. Facchi, and S. Pascazio. *Phys. Rev. Lett.*, **89**, 080401 (2002)

<sup>5</sup> J. Franson, B. Jacobs, and T. Pittman. *Phys. Rev. A*, **70**, 062302 (2004).

<sup>6</sup> L. Zhou, S. Yang, Y.-X. Liu, C. P. Sun, and F. Nori. *Phys. Rev. A*, **80**, 062109 (2009).

<sup>7</sup> S. Zhang, X.-Q. Shao, L. Chen, Y.-F. Zhao, and K.-H. Yeon. *J. Phys. B*, **44**, 075505 (2011).

<sup>8</sup> G. de Lange, Z. H. Wang, D. Ristè, V. V. Dobrovitski, and R. Hanson. *Science*, **330**, 60 (2010).

<sup>9</sup> T. Schröder, F. Gädeke, M. J. Banholzer, and O. Benson. *New J. Phys.*, **13**, 055017 (2011).

- <sup>10</sup> I. Aharonovich, S. Castelletto, D. Simpson, C.-H. Su, A. D. Greentree, and S. Prawer. *Rep. Prog. Phys.*, **74**, 076501 (2011).
- <sup>11</sup> T. D. Ladd, F. Jelezko, R. Laflamme, Y. Nakamura, C. Monroe, and J. L. O'Brien. *Nature*, **464**, 7285 (2010).
- <sup>12</sup> E. Togan, Y. Chu, A. S. Trifonov, L. Jiang, J. Maze, L. Childress, M. V. G. Dutt, A. S. Soerensen, P. R. Hemmer, A. S. Zibrov, and M. D. Lukin, *Nature*, **466**, 730 (2010).
- <sup>13</sup> H. Bernien, B. Hensen, W. Pfaff, G. Koolstra, M. S. Blok, L. Robledo, T. H. Taminiau, M. Markham, D. J. Twitchen, L. Childress, and R. Hanson, *arXiv*: 1212.6136 (2012).
- <sup>14</sup> L. T. Hall, G. C. G. Beart, E. A. Thomas, D. A. Simpson, L. P. McGuinness, J. H. Cole, J. H. Manton, R. E. Scholten, F. Jelezko, J. Wrachtrup, S. Petrou, and L. C. L. Hollenberg. *Sci. Rep.*, **2**, 401 (2012).
- <sup>15</sup> J. Wolters, A. W. Schell, G. Kewes, N. Nüsse, M. Schoengen, H. Döschner, T. Hannappel, B. Löchel, M. Barth, and O. Benson. *Appl. Phys. Lett.*, **97**, 141108 (2010).
- <sup>16</sup> J. Wolters, G. Kewes, A. W. Schell, N. Nüsse, M. Schoengen, B. Löchel, T. Hanke, R. Bratschitsch, A. Leitenstorfer, T. Aichele, and O. Benson. *Phys. Stat. Sol. (B)*, **249**, 918 (2012).
- <sup>17</sup> T. van der Sar, J. Hagemeyer, W. Pfaff, E. C. Heeres, S. M. Thon, H. Kim, P. M. Petroff, T. H. Oosterkamp, D. Bouwmeester, and R. Hanson. *Appl. Phys. Lett.*, **98**, 193103 (2011).
- <sup>18</sup> A. W. Schell, G. Kewes, T. Hanke, A. Leitenstorfer, R. Bratschitsch, O. Benson, and T. Aichele. *Opt. Express*, **19**, 7914 (2011).
- <sup>19</sup> R. Kolesov, B. Grotz, G. Balasubramanian, R. J. Stöhr, A. A. L. Nicolet, P. R. Hemmer, F. Jelezko, and J. Wrachtrup. *Nature Phys.*, **5**, 470 (2009).
- <sup>20</sup> F. Jelezko and J. Wrachtrup. *Phys. Stat. Sol. a*, **203**, 3207 (2006).
- <sup>21</sup> J. R. Maze, A. Gali, E. Togan, Y. Chu, A. Trifonov, E. Kaxiras, and M. D. Lukin, *New J. Phys.* **13**, 025025 (2011).
- <sup>22</sup> C. Santori, D. Fattal, and Y. Yamamoto. *Single-photon Devices and Applications*. (WILEY-VCH, Weinheim, 2010).
- <sup>23</sup> J. Wrachtrup and F. Jelezko. *J. Physics: Condens. Matter*, **18**, 807 (2006).
- <sup>24</sup> F. Shi, X. Rong, N. Xu, Y. Wang, J. Wu, B. Chong, X. Peng, J. Kniepert, R.-S. Schoenfeld, W. Harneit, M. Feng, and J. Du. *Phys. Rev. Lett.*, **105**, 040504 (2010).
- <sup>25</sup> P. C. Maurer, J. R. Maze, P. L. Stanwix, L. Jiang, A. V. Gorshkov, A. A. Zibrov, B. Harke, J. S. Hodges, A. S. Zibrov, A. Yacoby, D. Twitchen, S. W. Hell, R. L. Walsworth, and M. D. Lukin. *Nature Phys.*, **6**, 912 (2010).
- <sup>26</sup> C. Santori, P. Tamarat, P. Neumann, J. Wrachtrup, D. Fattal, R. Beausoleil, J. Rabeau, P. Olivero, A. Greentree, S. Prawer, F. Jelezko, and P. Hemmer. *Phys. Rev. Lett.*, **97**, 247401 (2006).
- <sup>27</sup> N. Manson, J. Harrison, and M. Sellars. *Phys. Rev. B*, **74**, 104303 (2006).



## SUPPLEMENTARY INFORMATION

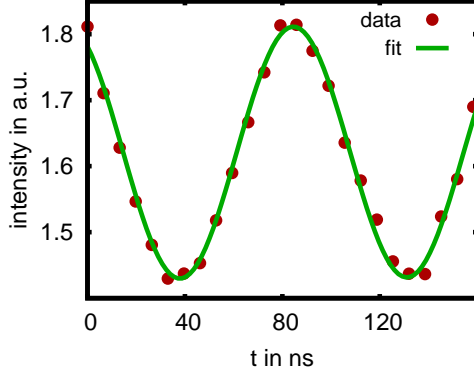


FIG. 6. Measured Rabi oscillations. A resonant microwave pulse of length  $t$  is applied and the fluorescence intensity recorded. The solid line is a fit to the data. MW power was slightly adjusted for the Zeno experiment to reach  $\Omega = 80$  ns.

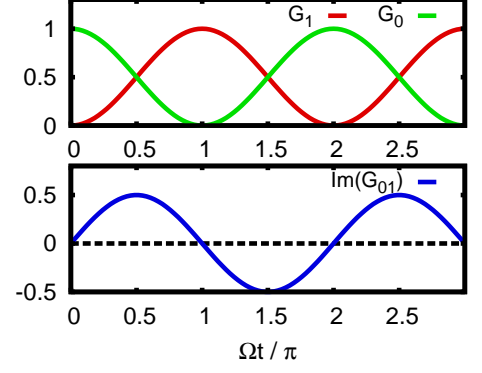


FIG. 7. Calculated Rabi oscillations of an ideal two level system without damping. Top: Calculated  $G_0(t)$  and  $G_1(t)$  occupation during a  $3\pi$  microwave pulse when starting with  $G_0(0) = 1$ . Bottom: The corresponding microscopic polarization  $G_{01}(t)$  reaches its maximal values at  $\Omega t = (n + 1/2)\pi$ . Then, a projective measurement most efficiently inhibits the dynamics.

The time derivatives of the level populations (cf. main text Fig. 3) and the quantum mechanic polarization between the ground states  $G_{01}(t)$  are given by Eqn. (1-6). Here,  $\Omega(t)$  is the time dependent MW Rabi frequency, which is equal to  $\Omega$  during the MW pulses and zero else. The excitation rate is modulated in a similar manner. Here we assume the switch-on to be of Gaussian shape with a HWHM of 2.5 ns, which is consistent with the measured slope of the used AOM. The pulsed laser is simulated by a 1 ns long interval of  $k_{exc} = 2.5/\text{ns}$ . The equations were numerically solved using Wolfram Mathematica, while initial values  $G_0(0)$  and  $G_1(0)$ , i.e.  $\tilde{G}_0$  and  $\tilde{G}_1$  were obtained to be self consistent.

$$\dot{E}_0(t) = k_{exc}(t) [\alpha G_0(t) + \beta G_1(t)] - [k_{rad} + \beta k_S] E_0(t) \quad (1)$$

$$\dot{E}_1(t) = k_{exc}(t) [\alpha G_1(t) + \beta G_0(t)] - [k_{rad} + \alpha k_S] E_1(t) \quad (2)$$

$$\dot{G}_{01}(t) = -\frac{i}{2} \Omega(t) [G_1(t) - G_0(t)] - G_{01}(t) \left[ \frac{1}{T_2} + k_{exc}(t) \right] \quad (3)$$

$$\dot{G}_0(t) = -\text{Im} [\Omega(t) G_{01}(t)] - k_{exc}(t) G_0(t) + k_{rad} [\alpha E_0(t) + \beta E_1(t)] + k_{desh} S(t) \quad (4)$$

$$\dot{G}_1(t) = \text{Im} [\Omega(t) G_{01}(t)] - k_{exc}(t) G_1(t) + k_{rad} [\alpha E_1(t) + \beta E_0(t)] \quad (5)$$

$$\dot{S}(t) = k_S [\alpha E_1(t) + \beta E_0(t)] - k_{desh} S(t). \quad (6)$$